UNIVERSITY OF CALIFORNIA SAN DIEGO

A Protein Kinase A-Regulated Network Encodes Short- and Long-Lived Cellular Memory

A Thesis submitted in partial satisfaction of the requirements
for the degree Master of Science

in

Biology

by

Yutian Li

Committee in charge:

Professor Nan Hao, Chair
Professor Brian Zid, Co-Chair
Professor Jeff Hasty

2019

The Thesis of Yutian Li is approved, and it is acceptable in quality and form for publication on microfilm and electronically:

_____

_____

Co-Chair

_____

Chair

University of California San Diego

2019

TABLE OF CONTENTS

LIST OF FIGURES

LIST OF TABLES

ACKNOWLEDGEMENTS

I would like to acknowledge Professor Nan Hao for his support as the chair of my thesis committee. His guidance has proven to be invaluable. I would also like to acknowledge the Hao Lab members for helping me throughout my research. It is their support that helped me in an immeasurable way.

This thesis, in full, is currently being prepared for submission for publication of the material. Jiang, Yanfei; AkhavanAghdam, Zohreh; Li, Yutian; Zid, Brian; Hao, Nan. The thesis author was the coauthor of this material.

ABSTRACT OF THE THESIS

A Protein Kinase A-Regulated Network Encodes Short- and Long-Lived Cellular Memory

by

Yutian Li

Master of Science in Biology

University of California San Diego, 2019

Professor Nan Hao, Chair
Professor Brian Zid, Co-Chair

In plants, bacteria, flies, and even humans, prior exposure to a previous mild stress allows the system to adapt better to a severe stress in the future, indicating that the concept of a "cellular memory" of previous stressful events might be a general feature of biological systems. In yeast, the protein kinase A (PKA)-mediated general stress response functions to respond to and store memories of prior stress exposure, which is required for resistance against future stressful conditions. Using microfluidics and time-lapse microscopy, we analyzed how cellular memory

of stress adaptation is dynamically encoded in single yeast cells. We found that the memory effect on future stress adaptation is biphasic, consisting of a short-lived component mediated by trehalose metabolism and a long-lasting component mediated by a transcriptional response and stabilized by messenger ribonucleoprotein granules. These two components could be selectively induced by different dynamics of priming inputs. Computational modeling further revealed how the PKA-mediated regulatory network could encode the information of previous stimuli into distinct memory dynamics. This biphasic memory-encoding scheme, analogous to innate and adaptive immune responses in mammals, might represent a general strategy to prepare for future challenges in rapidly changing environments.

Introduction

History-dependent cellular behaviors have been found in many organisms (Durrant & Dong, 2004; Hilker, et al., 2016; Lou & Yousef, 1997; Matsumoto, Hamada, Takahashi, Kobayashi, & Ohnishi, 2007; Netea, Latz, Mills, & O'Neill, 2015; Schenk, et al., 2000; Scholz, Franz, & Heberlein, 2005). For instance, it has been long established in the field of plant physiology that plant cells, once primed by mild stresses or chemical compounds, could obtain enhanced resistance to various future diseases and abiotic stresses (Conrath, et al., 2006; Savvides, Ali, Tester, & Fotopoulos, 2016). Priming of macrophages with interferon-gamma significantly boosts their lipopolysaccharide responses against various pathogens and induces production of tumor necrosis factor (Gifford & Lohmann-Matthes, 1987; Hayes, Freeman, & Donnelly, 1995). Similar phenomena have also been found in the yeast *Saccharomyces cerevisiae*, where a brief stress treatment can enhance cellular resistance to different types of future stresses (Berry & Gasch, Stress-activated Genomic Expression Changes Serve a Preparative Role for Impending Stress in Yeast, 2008; Guan, Haroon, Bravo, Will, & Gasch, 2012).

Cells survive rapidly changing environments through adaptation mediated by sophisticated signaling and gene regulatory networks. How these networks operate dynamically to process complex extracellular signals and elicit appropriate responses remains a challenging question (Behar & Hoffman, 2010; Levine, Lin, & Elowitz, 2013; Purvis & Lahav, 2013). In *Saccharomyces cerevisiae*, many different stresses, such as heat shock, osmotic stress, and carbon source starvation, can activate a general stress response mediated via protein kinase A (PKA) (Gasch, et al., 2000; Görner, et al., 1998; Martínez-Pastor, et al., 1996). Upon stress treatment, PKA is rapidly inhibited, leading to the activation of transcription factors (TFs) such as Msn2 and Msn4 and the induction of hundreds of stress responsive genes (Görner, et al., 1998; Hao & O'Shea,

Signal-dependent dynamics of transcription factor translocation controls gene expression, 2011; Martínez-Pastor, et al., 1996). Previous studies have demonstrated that the general stress response is not required to survive immediate stress threats; instead, its primary function is to maintain a cellular memory of prior stress exposures and enhance the acquired multi-stress resistance in preparation for future severe conditions (Berry & Gasch, 2008; Berry, et al., 2011; Guan, Haroon, Bravo, Will, & Gasch, 2012).

It is unclear how cells encode the memory to adapt to environmental change, in part due to difficulties in generating well-controlled sequential environmental changes in cell culture. Recent advances in microfluidic and single-cell imaging technologies allow both the precise control of extracellular conditions and single-cell response tracking over extended periods (Hansen, Hao, & O'Shea, High-throughput microfluidics to control and measure signaling dynamics in single yeast cells, 2015), facilitating analysis of the regulatory mechanisms underlying memory in stress responses. Using these technologies, we have employed yeast PKA-mediated general stress response as a model system to quantitatively investigate the molecular network that enables cells to encode memory of prior experience. We found that the memory shows two phases, a fast-decaying phase mediated by trehalose metabolism and a long-lasting phase mediated by stress-activated TFs and messenger ribonucleoprotein (mRNP) granules. Moreover, the memory dynamics can be modulated by priming inputs. Whereas a high amplitude transient input specifically induces the fast-decaying phase of memory, a prolonged input is needed to elicit the long-lasting memory effect. We further developed a computational model based on the molecular processes identified experimentally. Our model quantitatively revealed the regulatory scheme that encodes the information of previous environmental inputs into distinct memory dynamics,

implying a general strategy to optimize resource allocation and prepare for future challenges under rapidly changing environments.

Quantification of Memory Effect

In this study, we modified the channel design of an existing microfluidic device (Hao & O'Shea, Signal-dependent dynamics of transcription factor translocation controls gene expression, 2011) to include separate control of three media inlets, one for the priming input, one for the normal growth medium, and one for the stress treatment (Fig. 1A). To increase the experimental throughput, we further aligned four individual channels into a single device to enable simultaneous running of multiple experiments, each with its own cell population and stimulus condition. Using this device, we first exposed the cells to a pulse of priming input followed by a "break time" with the normal growth medium. We then treated these primed cells with a sustained environmental stress and evaluated their adaptation responses. The device was mounted on a time-lapse microscope to track the responses of a large number of single cells throughout the entire experiment.

For the priming input, we used a chemical genetics strategy in which we introduced analog-sensitive mutations into the PKA isoforms so that they remain fully functional but can be specifically inhibited by the small molecular inhibitor, 1-NM-PP1 (Bishop, et al., 2000). We have previously employed this strategy to control PKA activity and nuclear translocation of downstream TFs Msn2 and Msn4 (AkhavanAghdam, Sinha, Tabbaa, & Hao, 2016; Hansen & O'Shea, Promoter decoding of transcription factor dynamics involves a trade-off between noise and control of gene expression, 2013; Hao, Budnik, Gunawardena, & O'Shea, 2013; Hao & O'Shea, Signal-dependent dynamics of transcription factor translocation controls gene expression, 2011). This approach allows us to mimic an upstream signaling event that specifically activates the general stress response, but not other stress specific pathways. Moreover, combined with time-lapse microscopy and microfluidics, it enables us to generate precisely controlled temporal patterns of PKA

inhibition as priming inputs and evaluate their effects on cells' adaptation to the subsequent environmental stress.

For the subsequent stress treatment, we chose hyperosmotic stress (0.75M KCl) because the stress adaptation process in individual cells can be reliably quantified using a specific reporter, the stress-activated protein kinase Hog1, which we tagged with YFP. In response to osmotic stress, Hog1 rapidly translocates to the nucleus to induce an increase in intracellular osmolyte; once the osmolyte balance is restored and the cell recovers from the stress, Hog1 exits the nucleus (Brewster & Gustin, 2014). There is a strong correlation between the timing of Hog1 nuclear export and the restoration of cell volume (reflecting the turgor pressure recovery and cellular adaptation) (Muzzey, Gómez-Uribe, Mettetal, & Oudenaarden, 2009). Thus, the duration of Hog1 nuclear localization serves as a proxy for the time needed for the cell to recover from a stress treatment: a shorter duration represents a faster adaptation while a longer duration represents a slower adaptation. We observed that a 45-min priming input with 3 μM PKA inhibitor dramatically shortened the time needed to recover from hyperosmotic stress and this effect decays with increasing break times (Fig. 1B).

To quantify the effect of priming input and the dynamics of its decay, we measured and compared the durations of Hog1 nuclear translocation with and without the priming input (T_{primed}, $T_{unprimed}$) for each break time. For instance, the priming input with a 10-min break time decreased the adaptation time by 34.7% from 40 min to 26 min (Fig. 1C). We defined this percentage decrease in recovery time $\left(\frac{T_{unprimed} - T_{primed}}{T_{unprimed}}\right) \times 100\%$ as a quantitative measure of the "memory effect" and use it throughout our report.

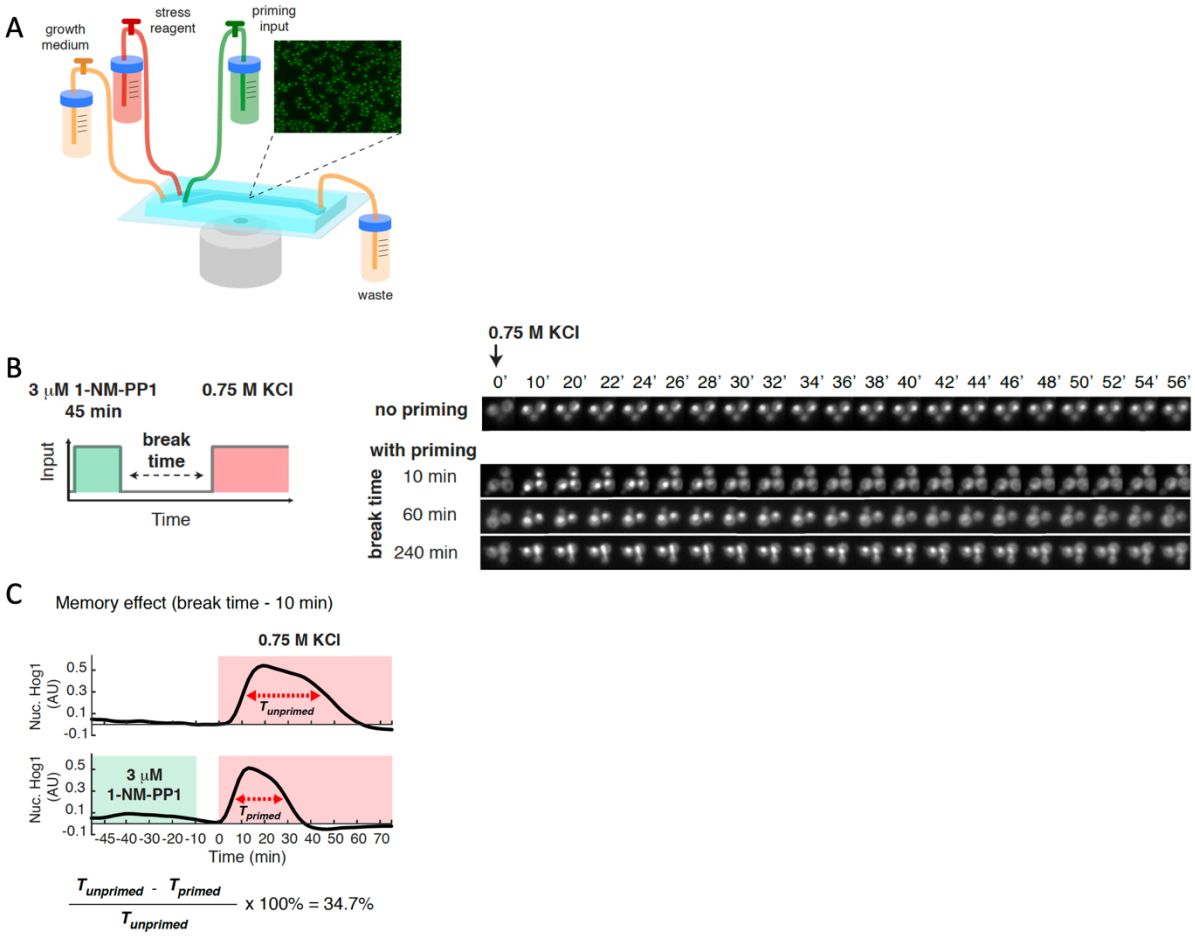

Figure 1. Measurement and quantification of memory effects as a function of the break time. (A) A diagram of the microfluidic system used in priming experiments. (B) Left: Schematic illustration of the priming experiments. Right Panel: Representative time-lapse images of Hog1 nuclear translocation in the priming experiments with different break times. (C) Results from a representative priming experiment to illustrate the quantification of memory effect. Time traces of Hog1 translocation in response to 0.75 M KCl (red shaded) without (top) or with (bottom) 45 min priming with 3 μM 1-NM-PP1 (green shaded) followed by 10 min break time. The duration of nuclear localization was quantified using the full width at half maximum in single cells.

Biphasic Cellular Memory of Yeast

We plotted the effect of the priming input (45 min, 3 μM 1-NM-PP1) as a function of break time and observed that the decay of memory effect is biphasic: About half of the memory effect was lost rapidly within 30 minutes, whereas the remaining memory effect plateaued until 90 minutes and then declined slowly (Fig. 2A). These biphasic memory dynamics were in contrast with the scenario where the memory is primarily mediated by expression of stress-resistance genes (Berry & Gasch, Stress-activated Genomic Expression Changes Serve a Preparative Role for Impending Stress in Yeast, 2008; Guan, Haroon, Bravo, Will, & Gasch, 2012), following an exponential decay trajectory as gene products are degraded during the break time. We termed the fast-decaying component "short-lived" memory and the longer-lasting component "long-lived" memory.

We next considered how changing the dynamics of priming inputs impacts cellular memory. To evaluate how the priming inputs duration influence memory dynamics, we decreased the input duration to 15 min and observed that cells only exhibited short-lived memory (Fig. 2B). When cycloheximide was added to inhibit protein synthesis during the priming experiment, short-term memory was not affected (Fig. 2C), suggesting that short-term memory is not gene expression-dependent, but may be mediated by metabolites or post-translational protein modifications.

To examine the effect of input amplitude, we treated cells with a reduced dosage of inhibitor (0.75 μM), which causes partial inhibition of PKA. (Hao, Budnik, Gunawardena, & O'Shea, 2013; Hao & O'Shea, Signal-dependent dynamics of transcription factor translocation controls gene expression, 2011). Under this condition, short-term memory and the plateau phase were both abolished (Fig. 2D), and cells displayed a slow decay trajectory. We also added

cycloheximide under this condition and found that the memory effect was dramatically diminished (Fig. 2E), demonstrating that this slowly decaying memory is mediated by gene expression.

In conclusion, the short-lived and long-lived components of cellular memory can be dissected by modulating the amplitude and duration of priming inputs and may be mediated by different molecular processes. Short-lived memory might be mediated through a fast translation-independent process, whereas an input duration-dependent slow gene expression process mediates the long-lasting memory, which could be further stabilized by another input amplitude-dependent mechanism. The three types of priming inputs are here referred to as: “high-amplitude prolonged” (3 μM 1-NM-PP1, 45 min); “high-amplitude transient” (3 μM, 15 min); and “low-amplitude prolonged” (0.75 μM, 45 min).

.

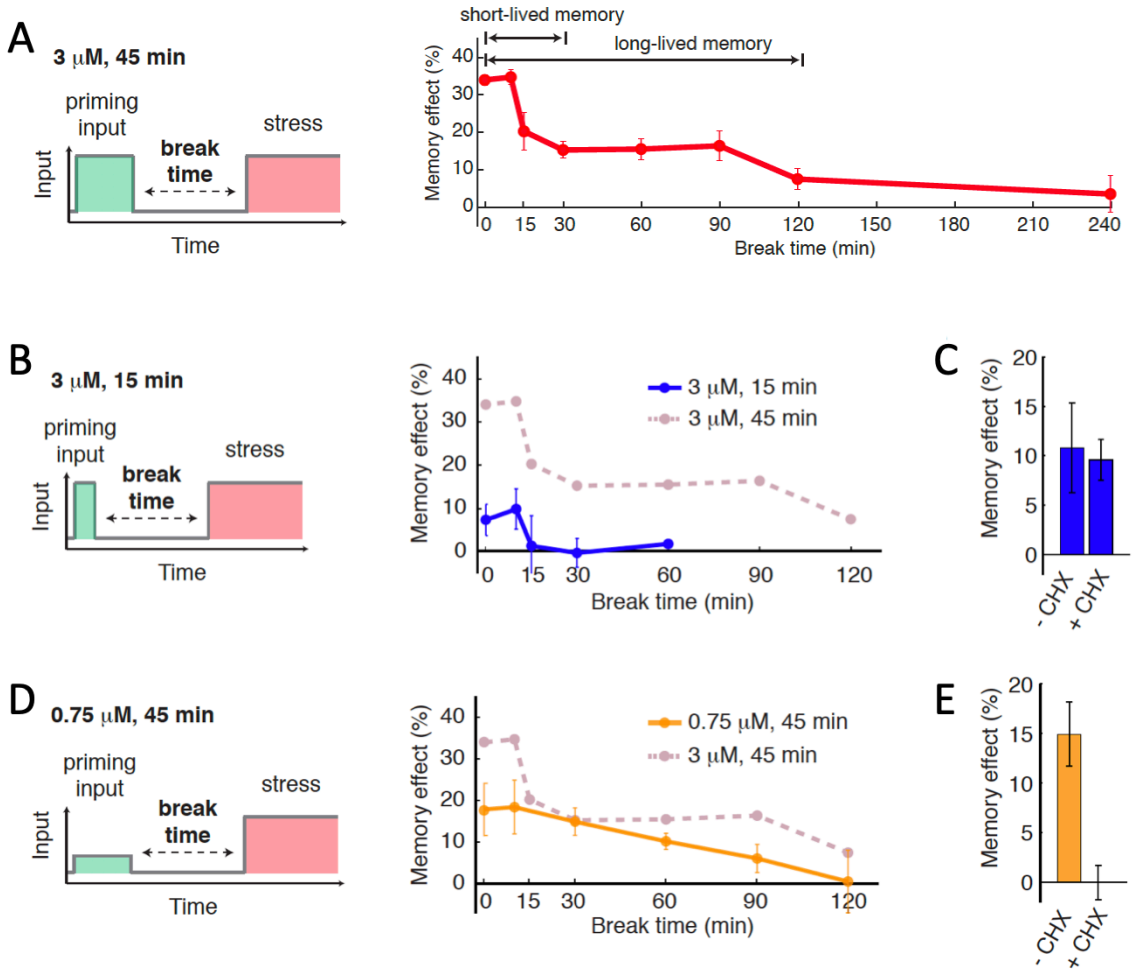

Figure 2. Biphasic memory effect can be dissected by different priming inputs.
(A) Biphasic memory dynamics in response to the high-amplitude prolonged priming input. The dynamics of memory effect in response to (B) the high-amplitude transient (15 min, 3 μM 1-NM-PP1) or (D) low-amplitude prolonged priming input (45 min, 0.75 μM 1-NM-PP1). Dashed line in dark pink represents memory dynamics from A and is included for comparison. Bar graph shows the memory effects in response to the indicated priming input with or without 10 mg/mL cycloheximide treatment (CHX) in response to the high-amplitude transient (C) or low-amplitude prolonged priming input (E). Data points are averages of at least three independent experiments. Error bars – standard error of the mean (SEM).

Trehalose Metabolism-Mediated Short-Lived Memory

To determine the molecular process that mediates short-lived memory, we systematically examined 5 known or putative PKA targets (Gph1, Ctt1, Nth1, Gcy1, and Tps1) that are regulated by PKA-dependent phosphorylation and are involved in metabolic or stress-response pathways (Hwang, Tugendreich, & Fletterick, 1989; Schepers, Zeebroeck, Pinkse, Verhaert, & Thevelein, 2012; Trevisol, Panek, De Mesquita, & Eleutherio, 2014). Among these PKA targets, Tps1 deletion abolished the fast-decaying component of memory (Fig. 3B). Note that the *tps1*Δ *hxk2*Δ strain was used because *tps1*Δ is unable to grow on glucose, but this growth is restored in a *tps1*Δ *hxk2*Δ double mutant (Hohmann, et al., 1993). The deletion of HXK2 alone does not affect the memory effect (Fig. 3B). Tps1 is a component of the trehalose synthase complex (De Virgilio, et al., 1993; Reinders, et al., 1997). Trehalose is a simple carbohydrate produced in many organisms that acts as membrane protectant and protein stabilizer to enhance cell survival under stressful conditions (Hounsa, Brandt, Thevelein, Hohmann, & Prior, 1998). In response to the high-amplitude prolonged input, Tps1 deletion abolished the fast-decaying component of memory, while long-lived memory remained unchanged (Fig. 3C). The intracellular trehalose level was rapidly induced in response to PKA inhibition and this induction was dependent on Tps1 (Fig. 3D).

To validate the central role of trehalose in short-term memory, we also manipulated its degradation. Nth1 is a trehalose degradation enzyme, the activity of which is regulated by PKA-dependent phosphorylation (Schepers, Zeebroeck, Pinkse, Verhaert, & Thevelein, 2012; Souza, De Mesquita, Panek, Silva, & Paschoalin, 2002). Deletion of Nth1 prolonged short-term memory (Fig. 3E). These results indicate that short-lived memory is mediated by PKA-regulated trehalose metabolism.

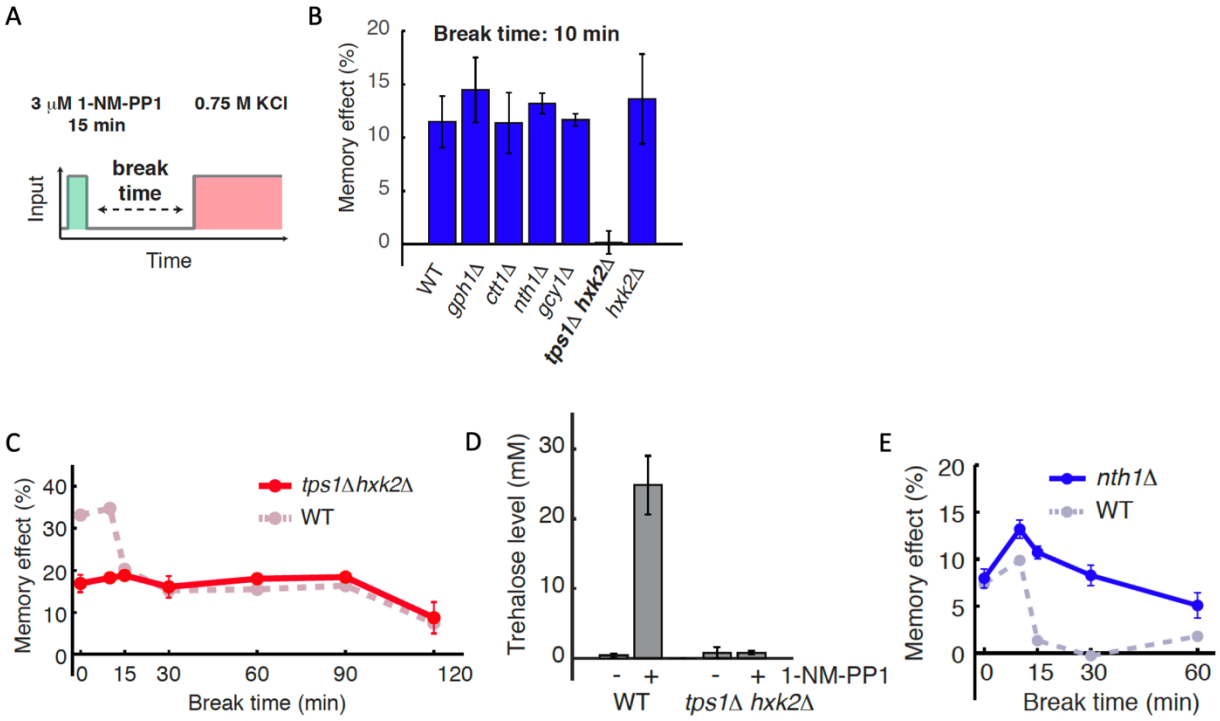

Figure 3. Identification of Tps1 in mediating short-lived memory.
(A) The schematic illustrating the treatment procedure of the priming experiment. (B) The bar graph shows the memory effects in response to the high-amplitude transient priming input (15 min, 3 μM 1-NM-PP1) with a 10 min break time in WT and mutant strains. (C) Memory dynamics in tps1Δ hxk2Δ. Dashed lines in dark pink show the memory dynamics in WT (from Fig. 2A). (D) Intracellular trehalose level in response to PKA inhibition. Trehalose levels were measured after a 20-min treatment of 3 μM 1-NM-PP1. (E) Memory dynamics in *nth1Δ* in response to the high-amplitude transient priming input (15 min, 3 μM 1-NM-PP1). Dashed lines in grey blue represent the memory dynamics in WT (from Fig. 2B) and are included in the plots for comparison.

PKA-regulated Transcription Factors Mediates Long-Lived Memory

Long-lived memory is mediated by gene expression: To determine the transcription factors (TFs) that induce this response, we systematically deleted PKA-regulated stress-responsive TFs (Gis1, Sko1, Hot1, Yap1, and Msn2/4) and examined their roles in mediating memory effect (Charizanis, Juhnke, Krems, & Entian, 1999; Görner, et al., 1998; Hinnebusch & Natarajan, 2002; Pascual-Ahuir, Posas, Serrano, & Proft, 2001; Proft, et al., 2001; Roosen, et al., 2005). We found that, whereas the deletion of Msn2/4 completely abolished long-term memory in response to the 45 minutes, 0.75 μM 1-NM-PP1 priming input (Fig. 4A), the mutant showed only a partial loss of memory in response to the 3 μM 1-NM-PP1 priming input (Fig. 4B), suggesting that another TF might play a compensatory role under this condition. As the deletion of Yap1 also dramatically diminished long-term memory in response to the 0.75 μM 1-NM-PP1 priming input (Fig. 4A), we generated the *msn2*Δ *msn4*Δ *yap1*Δ triple mutant and observed a complete loss of long-term memory in the triple mutant (Fig. 4B). These results identified Msn2/4 and Yap1 as primary TFs that mediate the long-lasting memory component. Moreover, we observed that the short-term and long-term memories are both abolished in the triple mutant (Fig. 4C). This loss of short-term memory in the triple mutant is consistent with previous studies (Hansen & O'Shea, 2013; Norbeck & Blomberg, 2000), which showed that the expression of *TPS1*, required for short-term memory, is completely dependent on the TFs deleted in the triple mutant.

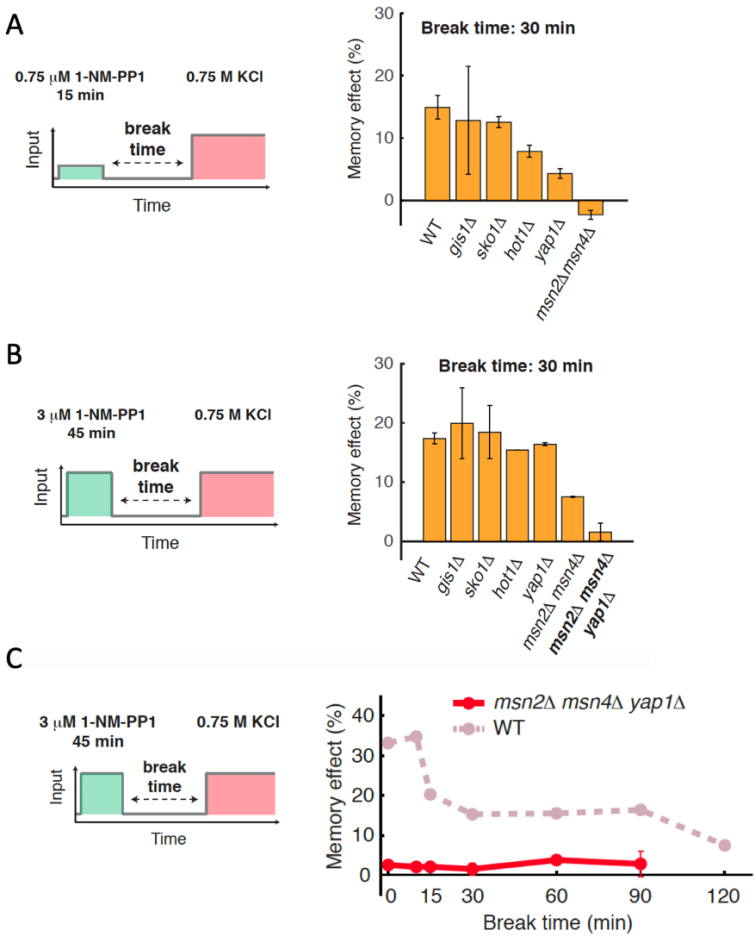

Figure 4. Identification of TFs Msn2/4 and Yap1 in mediating long-lived memory.
(A-B) Bar graph shows the memory effects in response to (A) the low-amplitude prolonged priming input (45 min, 0.75 μM 1-NM-PP1) or (B) the high-amplitude prolonged priming input (45 min, 3 μM 1-NM-PP1), with a 30 min break time in WT and mutant strains. (C) Memory dynamics in *msn2Δ msn4Δ yap1Δ*. Data points are averages of at least three independent experiments (error bars – SEM).

mRNP Granules Stabilizes Long-Lived Memory

Previous studies have revealed that, in response to stress or PKA inhibition, cells accumulate a number of stress-responsive gene mRNAs in cytoplasmic mRNP granules, called processing-bodies (PBs) and stress granules (SGs), which regulate mRNA translation, decay, and storage (Decker & Parker, 2012; Ramachandran, Shah, & Herman, 2011; Wang, et al., 2018; Zid & O'Shea, 2014). PKA regulates the formation of these mRNP granules by phosphorylating a PB scaffolding protein, Pat1 (Ramachandran, Shah, & Herman, 2011). To test whether mRNP granules contribute to the memory effect, we deleted PAT1. When Pat1 was deleted, the plateau phase of long-lived memory was abolished and the memory effect exhibited a continuous decay (Fig. 5B), indicating that PBs are required for maintaining the plateau phase. Some mRNAs in PBs can be stored in a translationally silenced state during stress and then return to translation via SGs upon stress removal (Buchan, Muhlrad, & Parker, 2008; Decker & Parker, 2012; Wang, et al., 2018). To determine the role of SGs in memory, we examined memory dynamics in the absence of the SG component Pub1 (Buchan, Muhlrad, & Parker, 2008). *pub1*Δ cells no longer exhibited the plateau phase, similar to *pat1*Δ (Fig. 5C). Therefore, the plateau phase of long-lived memory is dependent on the PB/SG-mediated mRNA storage pathway. Notably, *pat1*Δ and *pub1*Δ showed higher memory levels than those of WT for shorter break times (Fig. 5B and 5C, 15 - 30 mins), in agreement with the role of PBs/SGs in mRNA translational silencing in addition to storage. Furthermore, to confirm the localization of the mRNAs of stress responsive genes to mRNP granules induced by the priming input, we used the MS2 coat protein (MS2-CP) fused to GFP to visualize the mRNAs of two well-characterized Msn2/4-dependent genes, DCS2 and SIP18 in living yeast cells (AkhavanAghdam, Sinha, Tabbaa, & Hao, 2016; Haim-Vilmovsky, Gadir, Herbst, & Gerst, 2011; Hansen & O'Shea, Promoter decoding of transcription factor dynamics

involves a trade-off between noise and control of gene expression, 2013). Live-cell mRNA visualization revealed that, in response to PKA inhibition, the mRNAs of *DCS2* and *SIP18* formed foci that co-localized with PBs, and some distinct granules (Fig. 5D). Similar localization patterns have been observed for Msn2/4 targets, such as *GLC3* and *HXK1*, during glucose starvation and found to be coincided with poor protein production from these mRNAs during stress (Zid & O'Shea, 2014), suggesting that Msn2/4-dependent stress responsive mRNAs are translationally silenced and stored in mRNP granules in order to confer long-lasting stress resistance.

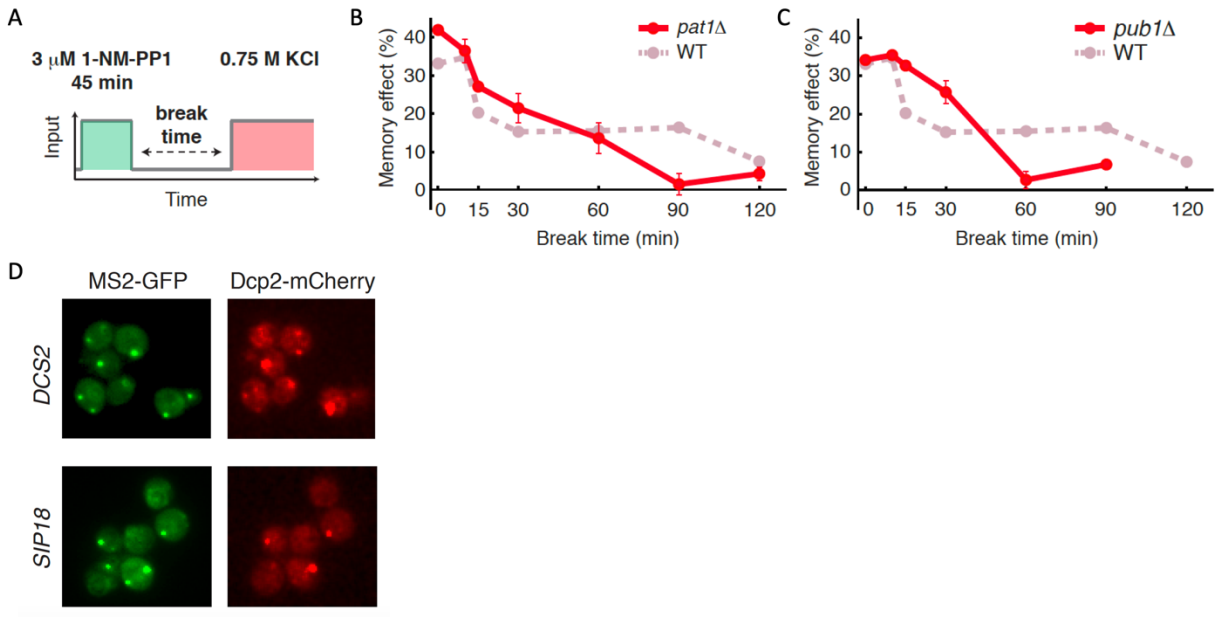

Figure 5. mRNP granules stabilizes long-lived memory.
(A) The schematic illustrating the treatment procedure of the priming experiments. (B-C) Memory dynamics in (B) *pat1Δ*, and (C) *pub1Δ*. Data points are averages of at least three independent experiments (error bars – SEM). (D) Co-localization of *DCS2* or *SIP18* mRNAs with PBs (Dcp2-mCherry) in response to 3 μM 1-NM-PP1. Foci formation was observed within 20 min of the input treatment. Representative images were acquired at 170 min.

Modeling reveals the network-mediated encoding of cellular memory

To quantitatively understand the dynamic encoding of memory, we constructed a model based on our experimental findings in which short-lived memory comprised of a fast process, where PKA-mediated phosphorylation regulated trehalose metabolism via Tps1 and Nth1 (Schepers, Zeebroeck, Pinkse, Verhaert, & Thevelein, 2012; Trevisol, Panek, De Mesquita, & Eleutherio, 2014), and long-lived memory consisted of two processes, a transcriptional response mediated by Msn2/4 and Yap1 (Görner, et al., 1998; Fernandes, Rodrigues-Pousada, & Struhl, 1997) and an mRNA storage process mediated by Pat1 (Decker & Parker, 2012). (Fig. 6A). With computationally obtained best-fit parameters, our model reproduced all the experimental data (Fig. 6B).

In particular, in our model, the high-amplitude transient input specifically induced the trehalose production process, generating the fast-decaying memory (Fig. 7A, top). The low-amplitude prolonged input induced the transcription response but did not induce mRNP granule formation, because the input was too weak, resulting in a slow exponential decay of the memory effect after input removal (Fig. 7A, middle). The high-amplitude prolonged input, however, lead to co-activation of both a fast trehalose production and a slow transcriptional response, including mRNA storage by mRNP granules. Once the transcriptional response was initiated, a portion of the newly synthesized stress resistance gene mRNAs was stored in mRNP granules via PKA regulation of Pat1. Upon input removal, these mRNAs were slowly released and translated, resulting in a long-lasting (up to ~90 minutes) memory plateau (Fig 7A, bottom). Consistent with the model, we observed that only the high-amplitude prolonged input strongly induced the formation of mRNP granules, as indicated by *DCS2* mRNA foci, whereas the high-amplitude transient input or low-amplitude prolonged input could not (Fig. 7A, insets), confirming that the

formation and function of mRNP granules depended on both the input amplitude and duration. Our model also reproduced the memory dynamics observed in the mutants of key regulatory factors, including *tps1*Δ, *pat1*Δ and *msn2*Δ *msn4*Δ *yap1*Δ (Fig. 8).

To further test our model, we used it to predict the memory dynamics in response to a combined pattern of priming input. Neither low-amplitude prolonged input nor high-amplitude transient input was able to induce the memory plateau phase, yet our model predicted that these two inputs, when applied sequentially, should be capable of generating a memory plateau phase that was Pat1 dependent (Fig. 7B, "Prediction"). In this scenario, the low-amplitude prolonged input would first produce a high level of mRNA, and then the subsequent high-amplitude transient input would induce mRNP granules to store newly synthesized mRNA, enabling the plateau phase. We experimentally tested these predictions, and in agreement with the model, we observed a memory plateau phase in response to the combined input (Fig. 7B, "Experiment"). This prediction is intriguing because it illustrates that the memory effect to the combined input is not simply the sum of the effects to the two single inputs (Fig. 7B, right panel, compare the purple versus light pink curves) and this is caused by the mRNP-dependent storage mechanism. Moreover, in the absence of Pat1, the plateau phase was abolished and the memory dynamics simply resembled the sum of memory effects to the two single inputs, consistent with the model prediction.

These results validated our model and demonstrated its predictive power. Given that the memory-encoding processes are kinetically separated, the model-guided analysis open a powerful possibility to rationally design patterns of priming input and reprogram the temporal order of regulatory processes for generating desired forms of memory dynamics.

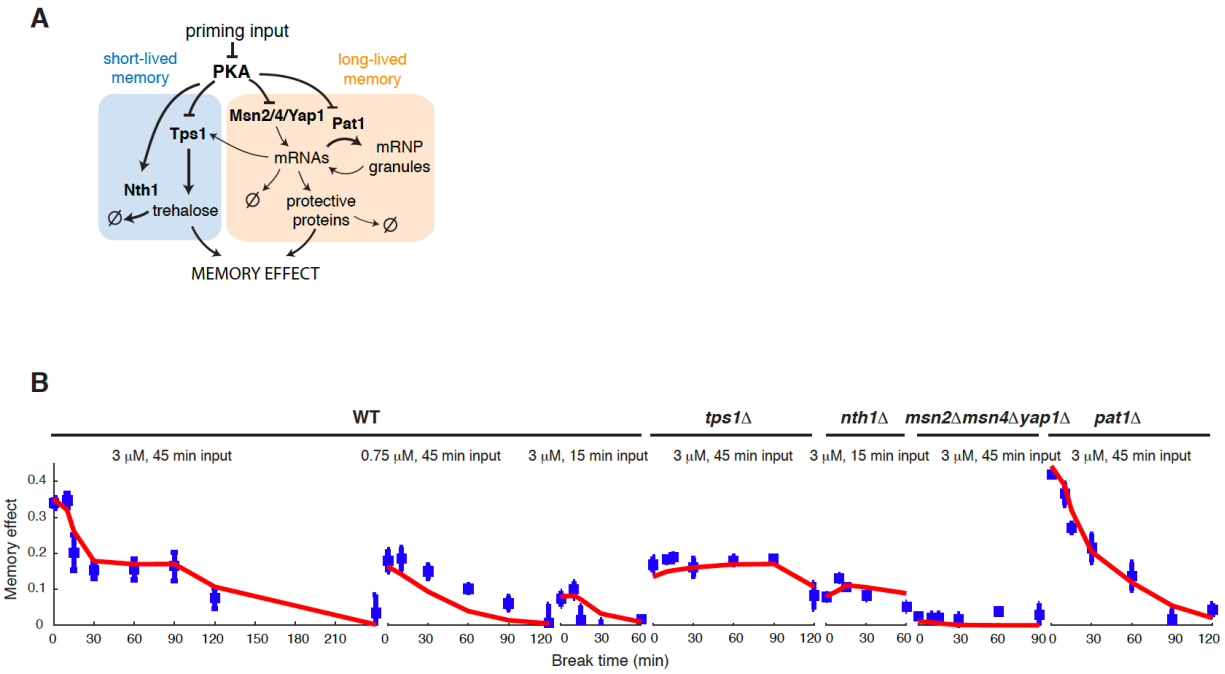

Figure 6. Computational modeling and data fitting.
(A) A diagram of the molecular network used in the model (B) Model fitting with all the experimental data. The blue squares show the experimental data with the error bars representing the standard errors. The red lines are the modeling results with the best-fit parameter values. Seven data sets were used for data fitting. The first three data sets are from Fig.2, which show the memory decay with three different inputs. The *tps1Δ, nth1Δ, msn2/4Δ yap1Δ*, and *pat1Δ* data are from Fig. 3-5. The fitting method is described in the materials and methods section.

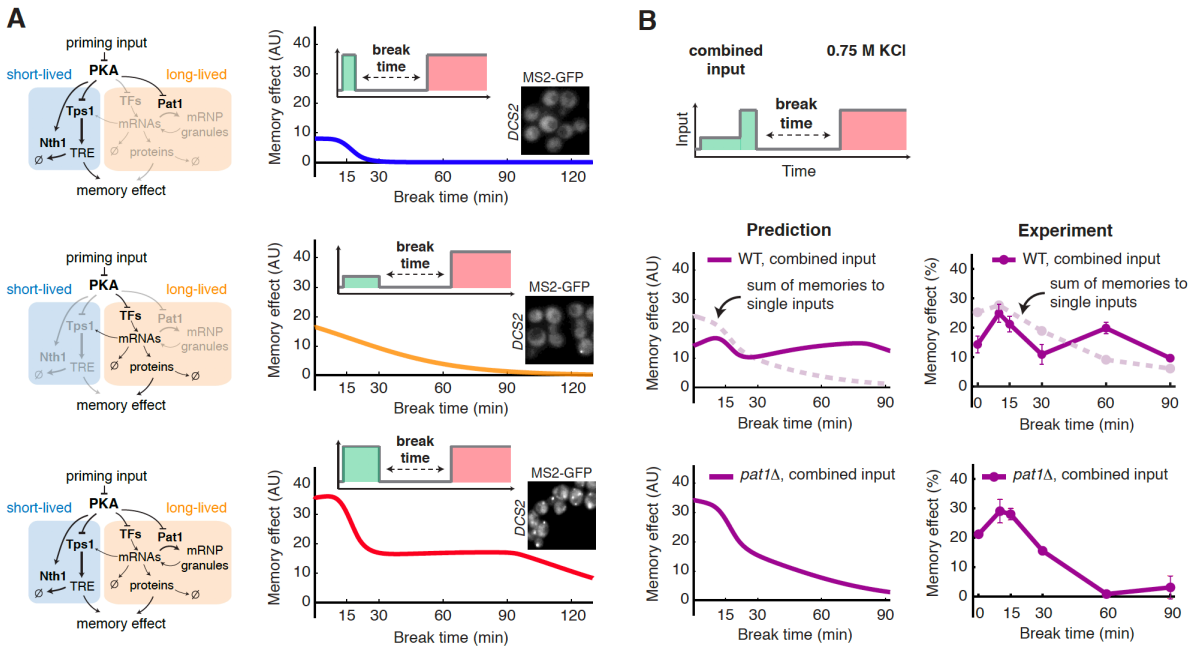

Figure 7. Modeling reveals the network-mediated encoding of cellular memory.
(A) Model simulation of memory dynamics in response to the high-amplitude transient (top), low-amplitude prolonged (middle) and high-amplitude prolonged (bottom) priming input, which activate the different pathways as depicted on left diagrams. The inserted cell images show the granule formation of DCS2 mRNA in response to indicated priming inputs. (B) Model prediction and validation. Two single inputs (45 min, 0.75 μM 1-NM-PP1 and 15 min, 3 μM 1-NM-PP1) were applied sequentially to produce the combined input. Model predictions and experimental data of memory dynamics in response to the combined inputs were shown for WT and pat1D. Dashed line in light pink represents the sum of memories to two single inputs from A and is included for comparison. Data points are averages of at least three independent experiments (error bars – SEM).

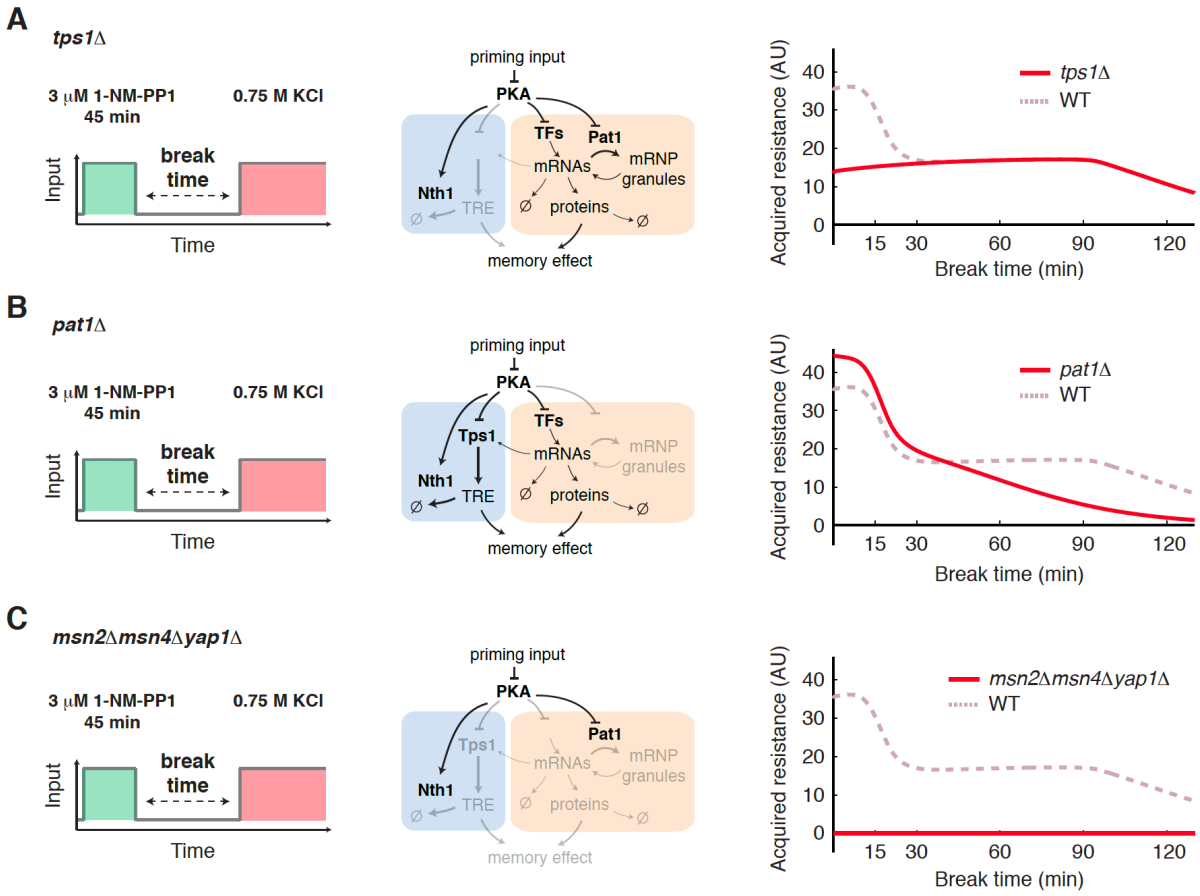

Figure 8. Computational modeling reproduces the modulation of memory dynamics in the absence of key regulatory factors.
(A) Model simulation of memory dynamics in the absence of Tps1. Left panel, the schematic illustrates the treatment procedure (45 min, 3 μM 1-NM-PP1). Middle panel, the diagram highlights the part of the network that remains activated in the absence of Tps1 (black – activated; light gray – not activated). Right panel, the plot shows the simulated dynamics of acquired stress resistance (corresponding to the memory effect in the data). Dashed line in dark pink represents the simulated dynamics of WT from Fig. 5C and is included in the plot for comparison. (B) Model simulation of memory dynamics in the absence of Pat1. (C) Model simulation of memory dynamics in the absence of Msn2/4 and Yap1.

Materials and Methods

Strain Construction

Standard methods for the growth, maintenance, and transformation of yeast and bacteria and for manipulation of DNA were used throughout. All *Saccharomyces cerevisiae* strains used in this study are derived from the W303 background (*MATa leu2-3,112 trp1-1 can1-100 ura3-1 ade2-1 his3-11,15 GAL+ psi+ ADE+*).

Microfluidics

The previously reported Y-shape microfluidic device (Hao & O'Shea, 2011; AkhavanAghdam, Sinha, Tabbaa, & Hao, 2016) with two inlets has been modified to accommodate three inlets on a single device and used in this study. The device fabrication and the setup of microfluidic experiments were performed as described previously (Hansen, Hao, & O'Shea, 2015; Hao & O'Shea, Signal-dependent dynamics of transcription factor translocation controls gene expression, 2011; AkhavanAghdam, Sinha, Tabbaa, & Hao, 2016; Hao, Budnik, Gunawardena, & O'Shea, 2013).

Time-lapse microscopy

All time-lapse microscopy experiments were performed using a Nikon Ti-E inverted fluorescence microscope with an Andor iXon X3 DU897 EMCCD camera and a Spectra X LED light source. A CFI Plan Apochromat Lambda DM 60X Oil Immersion Objective (NA 1.40 WD 0.13MM) was used for all experiments. Three positions were chosen for each microfluidics channel. For each position, phase contrast, YFP, mCherry, and iRFP images were taken sequentially every two minutes. When the acquisition of the image series started, cells loaded in

the microfluidic device were maintained in synthetic complete medium (SC, 2% dextrose) for the first five minutes before the introduction of 1-NM-PP1. Media input was switched manually between SC medium, SC medium with 1-NM-PP1 and SC medium with KCl at the indicated time points. The exposure and intensity settings for each fluorescence channel were set the same as that used in our earlier work (*21*).

For the priming experiments, cells were inoculated from a YPD plate into 2 ml SC liquid media two days before the experiment. On the second day, saturated cells were diluted by 1:20,000 into fresh SC media and grown overnight to reach OD = 0.6. These exponentially growing cells were diluted by 1:2 and grown for another 2 hours before being loaded into the microfluidic devices.

Image analysis

The images were processed using a custom MATLAB code for single-cell tracking and fluorescence quantification. The whole cell was segmented using the phase contrast images while the nucleus was segmented using the iRFP images. The cytoplasm was obtained by taking the difference of the whole cell and the nucleus. The nuclear to cytoplasmic ratios of Hog1-YFP were calculated using the mean fluorescence intensities of Hog1-YFP in the nucleus and in the cytoplasm. The ratios were subtracted by baseline which is the ratio right before KCl was introduced (close to 1) and then plotted against the time. The duration of Hog1 translocation for each condition was quantified using the full width at half maximum (FWHM) and used to calculate the memory effect for each break time, as illustrated in Fig. S1.

Trehalose assay

Trehalose level was measured using the trehalose assay kit (Megazyme). Using this assay, trehalose was converted into gluconate-6-phosphate, generating NADPH in a two-step reaction; the NADPH concentration can be determined by measuring the absorbance at 340 nm by spectrophotometry. To determine trehalose concentrations, 13 mL of yeast culture at OD≈0.5 was harvested and put on ice for 5 minutes before centrifuged for 5 min at 4 °C. Cells were then washed with 0.1 M phosphate buffer (pH 5.9) to remove glucose in media. After washing, cells were resuspended in 1 ml 0.25 M Na_2CO_3 solution and the cell densities (OD) was measured. Additional Na_2CO_3 solution was added to make the cell densities the same for 0 and 20 min samples. Samples (~1 mL) were boiled for 20 min to release intracellular trehalose. After cooling, the samples were centrifuged at 12 000 g for 3 min to remove cell debris. Two aliquots (300 μl) of supernatant were transferred to two new tubes with one tube for total glucose level and the other one for pre-existing glucose level. The following regents were then added to the cell lysates sequentially: 150 μl acetic acid (1 M), 650 ml distilled water, 100 μL imidazole buffer (2 M imidazole, 100 mM magnesium chloride and 0.02% w/v sodium azide; pH 7.0), 50 μL NADP 1 /ATP (12.5 mg/mL $NADP^+$ and 36.7 mg/mL ATP) and 10 μL suspension of HK/G-6-PDH (425 U/mL hexokinase and 212 U/mL glucose-6-phosphate dehydrogenase), 10 μL trehalase (490 U/mL). The mixtures were incubated at room temperature for 5 min for the reactions. Absorbance at 340 nm was recorded to determine the trehalose concentration in solution. To estimate the intracellular concentration, we assumed that cell density at OD=1 is $1x10^7$ cells/ml and yeast cell volume is 42 fl. Pre-existing glucose was determined in a control reaction without adding trehalase.

Live-cell mRNA visualization

The MS2-CP strains for mRNA visualization were constructed as described previously (Zid & O'Shea, 2014). The promoter and the coding region of genes of interest (e.g. *DCS2*) were amplified by PCR and then inserted into a template vector, which contains 12x MS2 loop sequences in the integration vector pRS305. The plasmid was linearized by EcoRV and integrated into W303 background yeast strain with PKA analog-sensitive mutations (NH084) at the *LEU2* locus. A plasmid that constitutively expresses MS2 coat proteins fused with GFP driven by *MYO2* promoter (Zid & O'Shea, 2014) was also integrated into the same strain at *HIS3* locus. To visualize the colocalization of mRNAs and PBs, a pRS304 plasmid that expresses *DCP2*-mCherry under the native *DCP2* promoter was integrated into the same strain at *TRP1* locus (NH0857).

To perform live-cell mRNA visualization, cells were cultured to OD 0.6 and then loaded into microfluidic devices for time-lapse microscopy. For each position, phase contrast, mCherry, GFP and iRFP images were taken sequentially every two minutes. When the image acquisition started, cells were maintained in SD media for the first five minutes to obtain a baseline for each fluorescence channel prior to the introduction of 3 μM 1-NM-PP1 treatment.

The exposure and intensity settings for each channel were set as follows: GFP 200 ms at 9% lamp intensity, mCherry 1s at 10% lamp intensity, and iRFP 300 ms at 15% lamp intensity.

Computational Modeling

Our model focuses on the PKA-dependent memory-encoding network, comprised of the experimentally-identified processes that regulate the levels of metabolites or proteins needed for enhancing stress adaptation, including trehalose and stress resistance gene products. The input of the model is the PKA inhibition signal (priming input). For the model output, we assume that the memory effect linearly depends on the sum of the amounts of trehalose and stress resistance gene products in most of the kinetic regimes, unless the substance concentrations reach extremely high levels. This assumption leaves out the explicit inclusion of the downstream Hog1 pathway in our model and simplifies our analysis. The network consists of three molecular processes, trehalose metabolism, stress resistance gene transcription and mRNP granule formation, all of which are PKA regulated.

For trehalose metabolism, PKA regulates both trehalose production and degradation by phosphorylating Tps1 and Nth1, respectively. More specifically, PKA-mediated phosphorylation inhibits Tps1 activity and enhances Nth1 activity based on the previous reports. Because the regulation is primarily through phosphorylation, we assume that it is a fast process. For stress resistance gene expression, PKA regulates mRNA transcription through transcription factors and regulates mRNA translation and degradation through mRNP granules. More specifically, the PKA inhibition input activates transcription factors and mRNP granules. Once the mRNP granules are activated, a portion of the newly synthesized mRNAs is stored in mRNP granules where their translation and degradation are paused. Upon input removal, these mRNAs are slowly released, resuming their translation and degradation. Because gene transcription is a multi-step process, we assume that it is a relatively slow process; in contrast, because PKA regulates mRNP granules through phosphorylation, we assume that it is a relatively fast process. It should be noted that the

level of Tps1 is also dependent on PKA-regulated gene expression, resulting in a connection between the trehalose metabolism pathway and the gene expression process. Based on the experimental observations, these three processes have different dependence on input amplitude and duration. Trehalose metabolism and mRNP granules can only be activated in response to high-amplitude inputs; by contrast, mRNA transcription can be induced by low-amplitude input, but a prolonged duration is needed.

Computational modeling and all the simulations were done using the MATLAB. The model contains 13 variables and 27 independent parameters. The function "lsqnonlin" was used for data fitting. The data of three dynamic inputs and three mutants (*tps1*Δ, *pat1*Δ, *msn2/4*Δ *yap1*Δ) were used for data fitting (Fig. 6). To highlight the role of mRNP granules, time points for long-lived memory plateau (Fig. 2A) were weighted by 20-fold for data fitting. Fitting starting with completely random guesses failed. Therefore, we first manually chose parameter values that can qualitatively capture the data and then used these manually-chosen parameters as the initial guesses for computational fitting. In order to overcome the local minimum, we also tested 10 random sets of initial guesses which are randomly chosen within 8 fold (1/8 to 8) of our first set of guesses and compared the squared norm of the residuals of the final fitting results and then selected the best-fit set of parameter values.

The initial conditions are provided in Table 1, reactions and rate constants are provided in Table 2.

Appendix

Model Equations:

$$\frac{d[TF_a]}{dt} = k_{11} \cdot [TF_i] - \frac{k_{12} \cdot PKA^4}{{KM_3}^4 + PKA^4} \cdot [TF_a]$$

$$\frac{d[TFi]}{dt} = -k_{11} \cdot [TF_i] + \frac{k_{12} \cdot PKA^4}{{KM_3}^4 + PKA^4} \cdot [TF_a]$$

$$\frac{d[Tps1RNA]}{dt} = \frac{k_{14} \cdot [TF_a]^2}{KM_8^2 + [TF_a]^2} + k_{15} - k_{16} \cdot [Tps1_{RNA}]$$

$$\frac{d[Tps1protein]}{dt} = k_{17} \cdot [Tps1RNA] - k_{13} \cdot [Tps1protein]$$

$$\frac{d[Nth1_a]}{dt} = \frac{k_1 \cdot PKA \cdot [Nth1_i]}{KM_4 + [Nth1_i]} - \frac{k_2 \cdot [Nth1_a]}{KM_6 + [Nth1_a]}$$

$$\frac{d[Nth1i]}{dt} = \frac{-k_1 \cdot PKA \cdot [Nth1_i]}{KM_4 + [Nth1_i]} + \frac{k_2 \cdot [Nth1_a]}{KM_6 + [Nth1_a]}$$

$$\frac{d[Trehalose]}{dt} = \frac{k_{19} \cdot {KM_7}^4}{KM_7^4 + PKA^4} \cdot [Tre6P] \cdot [Tps1protein] - \frac{k_{18} \cdot [Nth1_a]^4}{{KM_9}^4 + [Nth1_a]^4} \cdot [Trehalose]$$

$$\frac{d[Tre6P]}{dt} = \frac{-k_{19} \cdot {KM_7}^4}{{KM_7}^4 + PKA^4} \cdot [Tre6P] \cdot [Tps1protein]$$

$$\frac{d[Pat1_a]}{dt} = -k_4 \cdot [Pat1_a] + \frac{k_3 \cdot {KM_1}^4}{{KM_1}^4 + PKA^4} \cdot [Pat1_i] - (1 - PKA) \cdot k_6 \cdot [mRNAs] \cdot [Pat1_a] + \frac{k_5 \cdot [mRNPs]}{KM_2 + [mRNPs]}$$

$$\frac{d[Pat1_i]}{dt} = k_4 \cdot [Pat1_a] - \frac{k_3 \cdot {KM_1}^4}{{KM_1}^4 + PKA^4} \cdot [Pat1_i]$$

$$\frac{d[mRNPs]}{dt} = (1 - PKA) \cdot k_6 \cdot [mRNAs] \cdot [Pat1_a] - \frac{k_5 \cdot [mRNPs]}{KM_2 + [mRNPs]}$$

$$\frac{d[mRNAs]}{dt} = k_{10} \cdot [TF_a] - k_9 \cdot [mRNAs] - (1 - PKA) \cdot k_6 \cdot [mRNAs] \cdot [Pat1_a] + \frac{k_5 \cdot [mRNPs]}{KM_2 + [mRNPs]}$$

$$\frac{d[protein]}{dt} = k_8 \cdot [mRNAs] - k_7 \cdot [protein]$$

$$output = [Trehalose] + \frac{0.25 \cdot [protein]^2}{0.0625 + [protein]^2}$$

Table 1. Initial conditions of all species in the model.

Species	Initial conditions	Notes
TF_a	0	Active transcription factors, i.e. Msn2/4 and Yap1
TF_i	1	Active transcription factors
Tps1 mRNA	0.1	
Tps1 protein	1	
$Nth1_a$	0.2	Active Nth1
$Nth1_i$	0	Inactive Nth1
Trehalose	0	
Tre6P	0.35	Trehalose precursor, i.e. trehalose-6-P
$Pat1_a$	0	Active Pat1
$Pat1_i$	0.9	Inactive Pat1
mRNPs	0	mRNPs that stores mRNAs and induced by PKA inhibition
mRNAs	0	Stress responsive mRNAs induced by PKA inhibition
protein	0	Stress responsive proteins induced by PKA inhibition

Table 2. Best-fit parameter values used in the model.

Names	Parameters	Values
PKA activity	PKA	no inhibitor: 1 3μM1-NM-PP1: 0 0.75μM1-NM-PP1: 0.25
Transcription factor activation rate	k_{11}	0.009 min^{-1}
Transcription factor deactivation rate	k_{12}	50 min^{-1}
Transcription factor deactivation equilibrium constant	KM_3	1.3
Basal level of Tps1 mRNA transcription	k_{15}	0.01 min^{-1}
Tps1 mRNA transcription rate	k_{14}	0.4 min^{-1}
Tps1 mRNA degradation rate	k_{16}	0.05 min^{-1}
Tps1 translation rate	k_{17}	0.005 min^{-1}
Tps1 degradation rate	k_{13}	0.005 min^{-1}
Tps1 activation equilibrium constant	KM_6	0.01
Tps1 mRNA transcription equilibrium constant	KM_7	0.04
Nth1 activation rate	k_1	0.51 min^{-1}
Nth1 deactivation rate	k_2	0.5 min^{-1}
Nth1 activation equilibrium constant	KM_4	0.00001
Nth1 deactivation equilibrium constant	KM_5	0.00001
Trehalose production rate	k_{19}	0.02 min^{-1}
Trehalose decay rate (rate converting to downstream products)	k_{18}	0.41 min^{-1}
Trehalose decay equilibrium constant	KM_8	0.2
Pat1 activation rate	k_3	5 min^{-1}
Pat1 deactivation rate	k_4	0.5 min^{-1}
Pat1 activation equilibrium constant	KM_1	0.01
mRNPs formation rate	k_6	5 min^{-1}
mRNPs disassembly rate	k_5	0.01 min^{-1}
mRNPs disassembly equilibrium constant	KM_2	0.01
mRNA transcription rate	k_{10}	0.16 min^{-1}
mRNA degradation rate	k_9	0.02 min^{-1}
Stress resistance protein translation rate	k_8	3.2 min^{-1}
Stress resistance protein degradation rate	k_7	4 min^{-1}

Table 3. Strains used in this study.

Strain	Source	identifier
W303 MATa leu2-3,112 trp1-1 can1-100 ura3-1 ade2-1 his3-11,15 GAL+ psi+ ADE+, TPK1-M164G, TPK2-M147G, TPK3-M165G, NHP6a-iRFP-kanMX, MSN2-mCherry-TRP1, HOG1-YFP-HIS3	this study	NH0441
W303 MATa leu2-3,112 trp1-1 can1-100 ura3-1 ade2-1 his3-11,15 GAL+ psi+ ADE+, TPK1-M164G, TPK2-M147G, TPK3-M165G, NHP6a-iRFP-kanMX, MSN2-mCherry-TRP1, HOG1-YFP-HIS3, gph1::cgURA3	this study	NH0562
W303 MATa leu2-3,112 trp1-1 can1-100 ura3-1 ade2-1 his3-11,15 GAL+ psi+ ADE+, TPK1-M164G, TPK2-M147G, TPK3-M165G, NHP6a-iRFP-kanMX, MSN2-mCherry-TRP1, HOG1-YFP-HIS3, nth1::cgURA3	this study	NH0565
W303 MATa leu2-3,112 trp1-1 can1-100 ura3-1 ade2-1 his3-11,15 GAL+ psi+ ADE+, TPK1-M164G, TPK2-M147G, TPK3-M165G, NHP6a-iRFP-kanMX, MSN2-mCherry-TRP1, HOG1-YFP-HIS3, ctt1::cgURA3	this study	NH0566
W303 MATa leu2-3,112 trp1-1 can1-100 ura3-1 ade2-1 his3-11,15 GAL+ psi+ ADE+, TPK1-M164G, TPK2-M147G, TPK3-M165G, NHP6a-iRFP-kanMX, MSN2-mCherry-TRP1, HOG1-YFP-HIS3, gcy1::cgURA3	this study	NH0574
W303 MATa leu2-3,112 trp1-1 can1-100 ura3-1 ade2-1 his3-11,15 GAL+ psi+ ADE+, TPK1-M164G, TPK2-M147G, TPK3-M165G, NHP6a-iRFP-kanMX, MSN2-mCherry-TRP1, HOG1-YFP-HIS3, hxk2::cgLEU2	this study	NH0581
W303 MATa leu2-3,112 trp1-1 can1-100 ura3-1 ade2-1 his3-11,15 GAL+ psi+ ADE+, TPK1-M164G, TPK2-M147G, TPK3-M165G, NHP6a-iRFP-kanMX, MSN2-mCherry-TRP1, HOG1-YFP-HIS3, hxk2::cgLEU2, tps1::cgURA3	this study	NH0584
W303 MATa leu2-3,112 trp1-1 can1-100 ura3-1 ade2-1 his3-11,15 GAL+ psi+ ADE+, TPK1-M164G, TPK2-M147G, TPK3-M165G, NHP6a-iRFP-kanMX, MSN2-mCherry-TRP1, HOG1-YFP-HIS3, yap1::cgURA3	this study	NH0629
W303 MATa leu2-3,112 trp1-1 can1-100 ura3-1 ade2-1 his3-11,15 GAL+ psi+ ADE+, TPK1-M164G, TPK2-M147G, TPK3-M165G, NHP6a-iRFP-kanMX, MSN2-mCherry-TRP1, HOG1-YFP-HIS3, gis1::cgURA3	this study	NH0630
W303 MATa leu2-3,112 trp1-1 can1-100 ura3-1 ade2-1 his3-11,15 GAL+ psi+ ADE+, TPK1-M164G, TPK2-M147G, TPK3-M165G, NHP6a-iRFP-kanMX, MSN2-mCherry-TRP1, HOG1-YFP-HIS3, sko1::cgURA3	this study	NH0631

Table 3. Strains used in this study, continued

Strain	Source	identifier
W303 MATa leu2-3,112 trp1-1 can1-100 ura3-1 ade2-1 his3-11,15 GAL+ psi+ ADE+, TPK1-M164G, TPK2-M147G, TPK3-M165G, NHP6a-iRFP-kanMX, MSN2-mCherry-TRP1, HOG1-YFP-HIS, hot1:cgURA3	this study	NH0633
W303 MATa leu2-3,112 trp1-1 can1-100 ura3-1 ade2-1 his3-11,15 GAL+ psi+ ADE+, TPK1-M164G, TPK2-M147G, TPK3-M165G, NHP6a-iRFP-kanMX, HOG1-mCitrine(V163A)-HIS, msn4::cgTRP1, msn2::natMX, yap1::cgURA3	this study	NH0641
W303 MATa leu2-3,112 trp1-1 can1-100 ura3-1 ade2-1 his3-11,15 GAL+ psi+ ADE+, TPK1-M164G, TPK2-M147G, TPK3-M165G, NHP6a-iRFP-kanMX, MSN2-mCherry-TRP1, HOG1-YFP-HIS3, msn4::cgTRP1, msn2::natMX	this study	NH0442
W303 MATa leu2-3,112 trp1-1 can1-100 ura3-1 ade2-1 his3-11,15 GAL+ psi+ ADE+, TPK1-M164G, TPK2-M147G, TPK3-M165G, NHP6a-iRFP-kanMX, MSN2-mCherry-TRP1, HOG1-YFP-HIS3, pub1::cgURA3	this study	NH0688
W303 MATa leu2-3,112 trp1-1 can1-100 ura3-1 ade2-1 his3-11,15 GAL+ psi+ ADE+, TPK1-M164G, TPK2-M147G, TPK3-M165G, NHP6a-iRFP-kanMX, MSN2-mCherry-TRP1, HOG1-YFP-HIS3, pat1::cgURA3	this study	NH0689
W303 MATa leu2-3,112 trp1-1 can1-100 ura3-1 ade2-1 his3-11,15 GAL+ psi+ ADE+, TPK1-M164G, TPK2-M147G, TPK3-M165G, Nhp6a-iRFP:kanMX, MS2-CP-GFP-HIS3	this study	NH0812
W303 MATa leu2-3,112 trp1-1 can1-100 ura3-1 ade2-1 his3-11,15 GAL+ psi+ ADE+, TPK1-M164G, TPK2-M147G, TPK3-M165G, Nhp6a-iRFP:kanMX, MS2-CP-GFP-HIS3, DCS2-12xMS2-LEU2, DCP2-mCherry-TRP1	this study	NH0857
W303 MATa leu2-3,112 trp1-1 can1-100 ura3-1 ade2-1 his3-11,15 GAL+ psi+ ADE+, TPK1-M164G, TPK2-M147G, TPK3-M165G, Nhp6a-iRFP:kanMX, MS2-CP-GFP-HIS3, SIP18-12xMS2-LEU2, DCP2-mCherry-TRP1	this study	NH0858

This thesis, in full, is currently being prepared for submission for publication of the material. Jiang, Yanfei; AkhavanAghdam, Zohreh; Li, Yutian; Zid, Brian; Hao, Nan. The thesis author was the coauthor of this material.

References

AkhavanAghdam, Z., Sinha, J., Tabbaa, O. P., & Hao, N. (2016, September). Dynamic control of gene regulatory logic by seemingly redundant transcription factors. *Elife, 5*.

Behar, M., & Hoffman, A. (2010, December). Understanding the Temporal Codes of Intra-cellular Signals. *Curr Opin Genet Dev, 20*(6), 684-693.

Bennett, M. R., & Hasty, J. (2009, September). Microfluidic devices for measuring gene network dynamics in single cells. *Nat Rev Genet, 10*(9), 628-638.

Berry, D. B., & Gasch, A. P. (2008, Nov). Stress-activated Genomic Expression Changes Serve a Preparative Role for Impending Stress in Yeast. *Molecular Biology of The Cell, 19*(11), 4580-4587.

Berry, D. B., Guan, Q., Hose, J., Haroon, S., Gebbia, M., Heisler, L. E., Nislow, C., Giaever, G., Gasch, A. P. (2011, November). Multiple Means to the Same End: The Genetic Basis of Acquired Stress Resistance in Yeast. *PLoS Genet, 7*(11).

Bishop, A. C., Ubersax, J. A., Petsch, D. T., Matheos, D. P., Gray, N. S., Blethrow, J., Shimizu, E., Tsien, J. Z., Schultz, P. G., Rose, M. D., Wood, J. L., Morgan, D. O., Shokat, K. M. (2000, September). A chemical switch for inhibitor-sensitive alleles of any protein kinase. *Nature, 407*(6802), 395-401.

Brewster, J. L., & Gustin, M. C. (2014, September). Hog1: 20 years of discovery and impact. *Sci. Signal, 7*(343), re7.

Buchan, J., Muhlrad, D., & Parker, R. (2008, November). P bodies promote stress granule assembly in Saccharomyces cerevisiae. *J Cell Biol, 183*(3), 441-455.

Charizanis, C., Juhnke, H. D., Krems, B., & Entian, K.-D. (1999, June). The oxidative stress response mediated via Pos9/Skn7 is negatively regulated by the Ras/PKA pathway in Saccharomyces cerevisiae. *Mol Gen Genet, 261*(4-5), 740-752.

Conrath, U., Beckers, G., Flors, V., García-Agustín, P., Jakab, G., Mauch, F., Newman, M., Pieterse, C. M., Poinssot, B., Pozo, M. J., Pugin, A., Schaffrath, U., Ton, J., Wendehenne, D., Zimmerli, L., Mauch-Mani, B. (2006, October). Priming: Getting Ready for Battle. *Mol Plant Microbe Interact, 19*(10), 1062-1071.

De Virgilio, C., Bürckert, N., Bell, W., Jenö, P., Boller, T., & Wiemken, A. (1993, March). Disruption of TPS2, the gene encoding the 100-kDa subunit of the trehalose-6-phosphate synthase/phosphatase complex in Saccharomyces cerevisiae, causes accumulation of trehalose-6-phosphate and loss of trehalose-6-phosphate phosphatase activity. *Eur J Biochem, 212*(2), 315-323.

Decker, C. J., & Parker, R. (2012, September). P-Bodies and Stress Granules: Possible Roles in the Control of Translation and mRNA Degradation. *Cold Spring Harb Perspect Biol, 4*(9), a012286.

Durrant, W., & Dong, X. (2004, Sepyember). Systemic acquired resistance. *Annual Review of Phytopathology, 42*, 185-209.

Fernandes, L., Rodrigues-Pousada, C., & Struhl, K. (1997, December). Yap, a Novel Family of Eight bZIP Proteins in Saccharomyces cerevisiae with Distinct Biological Functions. *Mol Cell Biol, 17*(12), 6982-6993.

Görner, W., Durchschlag, E., Martinez-Pastor, M. T., Estruch, F., Ammerer, G., Hamilton, B., Ruis, H., Schüller, C. (1998, February). Nuclear localization of the C2H2 zinc finger protein Msn2p is regulated by stress and protein kinase A activity. *Genes Dev, 12*(4), 586-597.

Gasch, A. P., Spellman, P. T., Kao, C. M., Carmel-Harel, O., Eisen, M. B., Storz, G., Botstein, D., Brown, P. O. (2000, December). Genomic Expression Programs in the Response of Yeast Cells to Environmental Changes. *Molecular Biology of The Cell, 11*(12), 4241-4257.

Gifford, G. E., & Lohmann-Matthes, M.-L. (1987, January). Macrophages for Induction of Tumor Necrosis Factor Production by Bacterial Lipopolysaccharide. *Journal of the National Cancer Institute, 78*(1), 121-124.

Guan, Q., Haroon, S., Bravo, D. G., Will, J. L., & Gasch, A. P. (2012, October). Cellular Memory of Acquired Stress Resistance in Saccharomyces cerevisiae. *Genetics, 192*(2), 495-505.

Haim-Vilmovsky, L., Gadir, N., Herbst, R. H., & Gerst, J. E. (2011, December). A genomic integration method for the simultaneous visualization of endogenous mRNAs and their translation products in living yeast. *RNA, 17*(12), 2249-2255.

Hansen, A. S., & O'Shea, E. K. (2013, November). Promoter decoding of transcription factor dynamics involves a trade-off between noise and control of gene expression. *Mol Syst Biol, 9*, 704.

Hansen, A. S., Hao, N., & O'Shea, E. K. (2015, July). High-throughput microfluidics to control and measure signaling dynamics in single yeast cells. *Nature Protocols, 10*(8), 1181-1197.

Hao, N., & O'Shea, E. K. (2011, December). Signal-dependent dynamics of transcription factor translocation controls gene expression. *Nat Struct Mol Biol, 19*(1), 31-39.

Hao, N., Budnik, B. A., Gunawardena, J., & O'Shea, E. K. (2013, Jan). Tunable signal processing through modular control of transcription factor translocation. *Science, 339*(6118), 460-464.

Hayes, M. P., Freeman, S. L., & Donnelly, R. P. (1995, July). IFN-γ priming of monocytes enhances LPS-induced TNF production by augmenting both transcription and mRNA stability. *Cytokine, 7*(5), 427-435.

Hilker, M., Schwachtje, J., Baier, M., Balazadeh, S., Bäurle, I., Geiselhardt, S., Hincha, D. K., Kunze, R., Mueller-Roeber, B., Rolff, J., Romeis, T., Schmulling, T., Steppuhn, A., van Dongen, J., Whitchomb, S. J., Wurst, S., Zuther, E., Kopka, J. (2016, November). Priming and memory of stress responses in organisms lacking a nervous system. *Biological Reviews, 91*(4), 1118-1133.

Hinnebusch, A. G., & Natarajan, K. (2002, Feb). Gcn4p, a Master Regulator of Gene Expression, Is Controlled at Multiple Levels by Diverse Signals of Starvation and Stress. *Eukaryot Cell, 1*(1), 22-32.

Hohmann, S., Neves, M. J., de Koning, W., Alijo, R., Ramos, J., & Thevelein, J. M. (1993). The growth and signalling defects of the ggs1 (fdp1/byp1) deletion mutant on glucose are suppressed by a deletion of the gene encoding hexokinase PII. *Curr Genet, 23*(4), 281-289.

Hounsa, C.-G., Brandt, E., Thevelein, J., Hohmann, S., & Prior, B. A. (1998, March). Role of trehalose in survival of Saccharomyces cerevisiae under osmotic stress. *Microbiology, 144*(Pt 3), 671-680.

Hwang, P. K., Tugendreich, S., & Fletterick, R. J. (1989, Apr). Molecular analysis of GPH1, the gene encoding glycogen phosphorylase in Saccharomyces cerevisiae. *Mol Cell Biol, 9*(4), 1659-1666.

Levine, J. H., Lin, Y., & Elowitz, M. B. (2013, December). Functional roles of pulsing in genetic circuits. *Science, 342*(6163), 1193-1120.

Lou, Y., & Yousef, A. E. (1997, April). Adaptation to Sublethal Environmental Stresses Protects Listeria monocytogenes against Lethal Preservation Factors. *APPLIED AND ENVIRONMENTAL MICROBIOLOGY, 63*(4), 1252-1255.

Martínez-Pastor, M. T., Marchler, G., Schüller, C., Marchler-Bauer, A., Ruis, H., & Estruch, F. (1996, May). The Saccharomyces cerevisiae zinc finger proteins Msn2p and Msn4p are required for transcriptional induction through the stress response element (STRE). *EMBO J, 15*(9), 2227-2235.

Matsumoto, H., Hamada, N., Takahashi, A., Kobayashi, Y., & Ohnishi, T. (2007, April). Vanguards of Paradigm Shift in Radiation Biology: Radiation-Induced Adaptive and Bystander Responses. *Journal of Radiation Research, 48*(2), 97-106.

Muzzey, D., Gómez-Uribe, C. A., Mettetal, J. T., & Oudenaarden, A. v. (2009, July). A systems-level analysis of perfect adaptation in yeast osmoregulation. *Cell, 138*(1), 160-171.

Netea, M. G., Latz, E., Mills, K. H., & O'Neill, L. A. (2015, July). Innate immune memory: a paradigm shift in understanding host defense. *Nature Immunology , 16*(7), 675-679.

Norbeck, J., & Blomberg, A. (2000, January). The level of cAMP-dependent protein kinase A activity strongly affects osmotolerance andosmo-instigated gene expression changes in Saccharomyces cerevisiae. *Yeast, 16*(2), 121-137.

Pascual-Ahuir, A., Posas, F., Serrano, R., & Proft, M. (2001, October). Multiple Levels of Control Regulate the Yeast cAMP-response Element-binding Protein Repressor Sko1p in Response to Stress*. *J Biol Chem, 276*(40), 37373-37378.

Proft, M., Pascual-Ahuir, A., de Nadal, E., Ariño, J., Serrano, R., & Posas, F. (2001, March). Regulation of the Sko1 transcriptional repressor by the Hog1 MAP kinase in response to osmotic stress. *EMBO J, 20*(5), 1123-1133.

Purvis, J. E., & Lahav, G. (2013, February). Encoding and Decoding Cellular Information through Signaling Dynamics. *Cell, 152*(5), 945-956.

Ramachandran, V., Shah, K. H., & Herman, P. K. (2011, September). The cAMP-dependent protein kinase signaling pathway is a key regulator of P body foci formation. *Mol Cell, 43*(6), 973-81.

Reinders, A., Bürckert , N., Hohmann, S., Thevelein, J. M., Boller, T., Wiemken, A., & De Virgilio, C. (1997, May). Structural analysis of the subunits of the trehalose-6-phosphate synthase/phosphatase complex in Saccharomyces cerevisiae and their function during heat shock. *Mol Microbiol, 24*(4), 687-695.

Roosen, J., Engelen, K., Marchal, K., Mathys, J., Griffioen, G., Cameroni, E., Thevelein, J. M., De Virgilio, C., De Moor, B., Winderickx, J. (2005, February). PKA and Sch9 control a molecular switch important for the proper adaptation to nutrient availability. *Mol Microbiol, 55*(3), 862-880.

Savvides, A., Ali, S., Tester, M., & Fotopoulos, V. (2016, April). Chemical Priming of Plants Against Multiple Abiotic Stresses: Mission Possible? *Trends in Plant Science, 21*(4), 329-340.

Schenk, P. M., Kazan, K., Wilson, I., Anderson, J. P., Richmond, T., Somerville, S. C., & Manners, J. M. (2000, October). Coordinated plant defense responses in Arabidopsis revealed by microarray analysis. *Proc Natl Acad Sci U S A, 97*(21), 11655-11660.

Schepers, W., Zeebroeck, G. V., Pinkse, M., Verhaert, P., & Thevelein, J. M. (2012, December). In Vivo Phosphorylation of Ser21 and Ser83 during Nutrient-induced Activation of the Yeast Protein Kinase A (PKA) Target Trehalase. *J Biol Chem, 287*(53), 44130-44142.

Scholz, H., Franz, M., & Heberlein, U. (2005, August). The hangover gene defines a stress pathway required for ethanol tolerance development. *Nature, 436*(7052), 845-847.

Souza, A. C., De Mesquita, J. F., Panek, A. D., Silva, J. T., & Paschoalin, V. M. (2002, January). Evidence for a modulation of neutral trehalase activity by Ca2+ and cAMP signaling pathways in Saccharomyces cerevisiae. *Braz J Med Biol Res, 35*(1), 11-16.

Trevisol, E. T., Panek, A. D., De Mesquita, J. F., & Eleutherio, E. C. (2014, June). Regulation of the yeast trehalose–synthase complex by cyclic AMP-dependent phosphorylation. *Biochim Biophys Acta, 1840*(6), 1646-1650.

Wang, C., Schmich, F., Srivatsa, S., Weidner, J., Beerenwinkel, N., & Spang, A. (2018, January). Context-dependent deposition and regulation of mRNAs in P-bodies. *Elife, 7*(e29815).

Zid, B. M., & O'Shea, E. K. (2014, October). Promoter sequences direct cytoplasmic localization and translation of mRNAs during starvation in yeast. *Nature, 514*(7520), 117-121.